Inhibition Pathways of the Potent Organophosphate CBDP with Cholinesterases Revealed by X-ray Crystallographic Snapshots and Mass Spectrometry

ARTICLE *in* CHEMICAL RESEARCH IN TOXICOLOGY · JANUARY 2013

Impact Factor: 3.53 · DOI: 10.1021/tx3004505 · Source: PubMed

Chemical Research in Toxicology

Article

pubs.acs.org/crt

Inhibition Pathways of the Potent Organophosphate CBDP with Cholinesterases Revealed by X-ray Crystallographic Snapshots and Mass Spectrometry

Eugénie Carletti,[†,‡,§,∥] Jacques-Philippe Colletier,[†,‡,§] Lawrence M. Schopfer,[⊥] Gianluca Santoni,[†,‡,§,∥] Patrick Masson,[†,‡,§,∥,⊥] Oksana Lockridge,[⊥] Florian Nachon,*[,∥] and Martin Weik*[,†,‡,§,#]

[†]Institut de Biologie Structurale J.P. Ebel, Commissariat à l'Energie Atomique, 41, rue Jules Horowitz, F-38027 Grenoble, France

[‡]CNRS, UMR5075, F-38027 Grenoble, France

[§]Université Joseph Fourier, F-38000 Grenoble, France

[∥]Département de Toxicologie, Institut de Recherche Biomédicale des Armées, 24 avenue des Marquis du Grésivaudan, 38702 La Tronche, France

[⊥]Eppley Institute, University of Nebraska Medical Center, Omaha, Nebraska 68198-5950, United States

[#]ESRF, 6 rue Jules Horowitz, BP 220, 38043 Grenoble Cedex, France

Supporting Information

ABSTRACT: Tri-*o*-cresyl-phosphate (TOCP) is a common additive in jet engine lubricants and hydraulic fluids suspected to have a role in aerotoxic syndrome in humans. TOCP is metabolized to cresyl saligenin phosphate (CBDP), a potent irreversible inhibitor of butyrylcholinesterase (BChE), a natural bioscavenger present in the bloodstream, and acetylcholinesterase (AChE), the off-switch at cholinergic synapses. Mechanistic details of cholinesterase (ChE) inhibition have, however, remained elusive. Also, the inhibition of AChE by CBDP is unexpected, from a structural standpoint, i.e., considering the narrowness of AChE active site and the bulkiness of CBDP. In the following, we report on kinetic X-ray crystallography experiments that provided 2.7−3.3 Å snapshots of the reaction of CBDP with mouse AChE and human BChE. The series of crystallographic snapshots reveals that AChE and BChE react with the opposite enantiomers and that an induced-fit rearrangement of Phe297 enlarges the active site of AChE upon CBDP binding. Mass spectrometry analysis of aging in either $H_2{}^{16}O$ or $H_2{}^{18}O$ furthermore allowed us to identify the inhibition steps, in which water molecules are involved, thus providing insights into the mechanistic details of inhibition. X-ray crystallography and mass spectrometry show the formation of an aged end product formed in both AChE and BChE that cannot be reactivated by current oxime-based therapeutics. Our study thus shows that only prophylactic and symptomatic treatments are viable to counter the inhibition of AChE and BChE by CBDP.

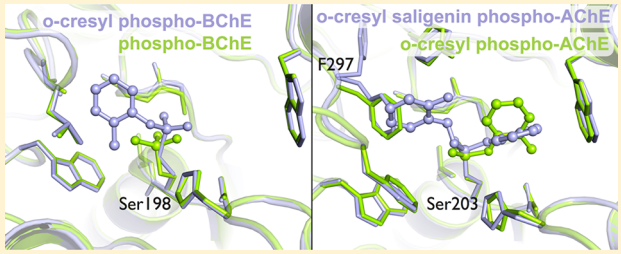

INTRODUCTION

Tri-*o*-cresyl phosphate (TOCP), a toxic isomer of tricresyl phosphate (TCP), is suspected to play an important role in aerotoxic syndrome. TCP is added to commercial jet engine lubricants for its antiwear and flame-retardant properties.[1−3] When oil seals in jet-airplanes leak, the cabin bleed-air becomes contaminated with TOCP. TOCP is inhaled and metabolized by liver microsomal cytochrome P450 and serum albumin into 2-(*o*-cresyl)-4*H*-1,3,2-benzodioxaphosphoran-2-one (CBDP), also called cresyl saligenin phosphate.[4−6]

CBDP is a bicyclic organophosphorus compound (OP), which irreversibly inhibits both human acetylcholinesterase (hAChE; EC 3.1.1.7) and butyrylcholinesterase (hBChE; EC 3.1.1.8).[7] hAChE is the enzyme responsible for the termination of nerve-impulse transmission at cholinergic synapses, and as such, it is the primary target of chemically synthesized OPs. hBChE is a structurally and functionally homologous enzyme that is present in the bloodstream (50 nM, in humans) and acts as a stoichiometric bioscavenger of OPs.[8] Irreversible inhibition of hAChE and hBChE by OPs generally proceeds in two steps; phosphylation of the catalytic serine with concomitant release of a leaving group, followed by dealkylation of the OP-enzyme adduct, a process also called aging. It is noteworthy that medical countermeasures to reactivate cholinesterases are only efficient against nonaged enzymes:[9] aged ChEs can indeed no longer be reactivated by oximes used as antidotes against OP poisoning.

hAChE and hBChE differ mostly by the amino acid distribution in their active site gorges, the former containing more aromatic residues than the latter. In particular, the replacement of two phenylalanine residues in the acyl-binding

Received: November 9, 2012
Published: January 22, 2013

pocket of hAChE, by a leucine and a valine in BChE, results in an enlargement of the pocket, thereby allowing accommodation of bulkier substrates and inhibitors and expanding the substrate specificity of hBChE as compared to that of hAChE.[10] Accordingly, hAChE and hBChE have repeatedly been reported to preferentially react with different OP stereoisomers.[11]

The ensemble of neurological symptoms associated with aerotoxic syndrome includes memory impairment and uncontrollable shaking.[12,13] It has been shown that CBDP inhibits esterase enzymes, notably the neuropathy target esterase[14,15] but also hBChE and hAChE.[7,16−18] In addition, other serine esterases are likely inhibited by CBDP and tyrosine residues in several proteins have been shown to be reactive toward CBDP. Inhibition of such proteins may participate in the pathogenesis of aerotoxic syndrome.

We earlier investigated the inhibition mechanisms of hAChE and hBChE by CBDP using a combination of kinetic measurements, mass spectrometry, and X-ray crystallography.[7] As shown in Scheme 1, the inhibition of hBChE by CBDP occurs in three steps.

Scheme 1. Reaction of CBDP with hBChE

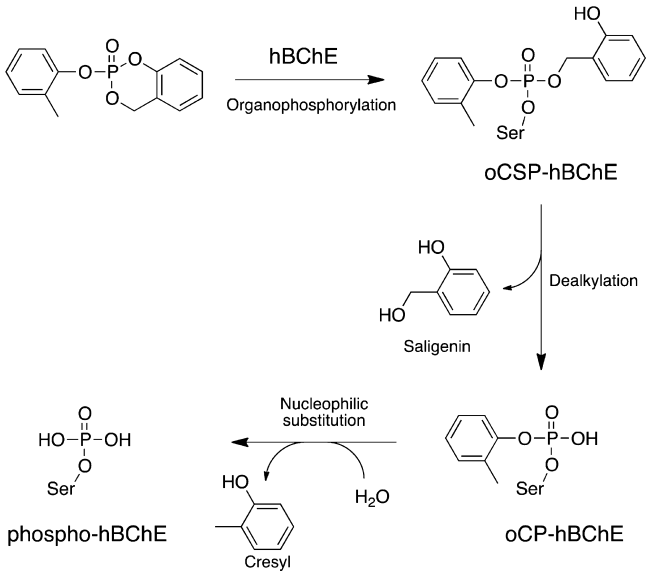

CBDP first forms a phosphorylserine conjugate of hBChE, with saligenin and *o*-cresyl as substituents (oCSP-hBChE). The first aging reaction corresponds to the release of the saligenin moiety, and results in the *o*-cresyl-phospho-BChE adduct (oCP-hBChE). A second aging reaction then occurs that allows the release of the *o*-cresyl moiety and yields phospho-hBChE, whose structure we reported already.[7] We also showed that the bimolecular rate constant of CBDP for hBChE is at least 10-fold higher than that for hAChE. CBDP is, in fact, one of the most potent BChE inhibitors reported to date (1.5×10^8 $M^{-1}\cdot min^{-1}$), suggesting that hBChE efficiently scavenges CBDP in the bloodstream. The reactivity of CBDP toward hAChE is in the same range as that exhibited by paraoxon, tabun, or soman (10^6–10^7 $M^{-1}\cdot min^{-1}$). It remains unclear, however, if hAChE and hBChE inhibition by CBDP proceeds in the same fashion, and whether the same intermediate states form.

Here, we provide a detailed description of mouse (m) AChE and human (h) BChE inhibition by CBDP, based on crystallographic snapshots of inhibition intermediate states and on mass spectrometry analyses. We show that mAChE inhibition by CBDP occurs in two steps and involves a transient enlargement of the acyl-binding pocket to allow accommodation of the bulky CBDP adduct. The resulting *o*-cresyl-phospho-mAChE is a stable OP-aged adduct that does not evolve further. In contrast, the *o*-cresyl-phospho-hBChE adduct represents an unstable, strained conformer of hBChE that undergoes a second aging reaction yielding a phospho-serine-hBChE adduct. CBDP inhibition of mAChE and hBChE involves a different stereoisomer of CBDP, occurs through different pathways, and yields a different end-conjugate.

EXPERIMENTAL PROCEDURES

Caution: *CBDP is a highly toxic organophosphorus compound. Handling requires suitable personal protection, training, and facilities. These requirements are the same as those for other poisonous organophosphorus compounds.*

Chemicals. CBDP was synthesized by Starks Associates Buffalo, NY, and provided by Dr. D. Lenz (USAMRICD, Aberdeen PG, MD) and Dr. Wolf Dettbarn (Vanderbilt University, Nashville, TN). A 0.1 M stock solution of CBDP in acetonitrile was stored at −20 °C and diluted in water on the day of the mass spectrometry or crystallography experiment. Pepsin (from porcine stomach mucosa) was purchased from Sigma (a member of the Sigma-Aldrich group, St. Louis, MO). ^{18}O-Water (99% ^{18}O) was purchased from ISOTEC (a member of the Sigma-Aldrich group). Chemical structures and reaction schemes were illustrated using the program ChemDraw (CambridgeSoft).

Production of Recombinant ChEs. Recombinant hBChE (L530stop) is a truncated monomer containing residues 1 to 529 but missing 45 C-terminal residues that include the tetramerization domain. Four of the nine carbohydrate attachment sites were deleted by site-directed mutagenesis. Mutagenesis of N486 resulted in glycosylation of N485, an asparagine that is not glycosylated in native hBChE so that the recombinant hBChE contains six N-linked glycans.[19] The recombinant hBChE gene was expressed in Chinese hamster ovary (CHO) cells, secreted into serum-free culture medium, and purified by affinity and ion-exchange chromatographies as described previously.[19]

The synthetic gene (GeneArt) coding for a truncated mutant of mAChE (L544Stop) was inserted into a pGS vector carrying the glutamine synthetase gene marker and expressed in Chinese hamster ovary (CHO)-K1 cells. The cells were maintained in serum-free Ultraculture Medium (BioWhittaker, Walkersville, MD) and transfected using DNA−calcium phosphate coprecipitation. Transfected clones were selected by incubation in media containing methionine sulfoximine. The mouse enzyme, secreted into the culture medium, was purified by affinity chromatography and ion-exchange chromatography using a protocol identical to that described for the recombinant human enzyme.[20] The enzyme was concentrated to 14 mg/mL using a Centricon-30 ultrafiltration microconcentrator (30000 MW cutoff, Amicon, Millipore, Billerica, MA) in 10 mM MES buffer at pH 6.5.

Crystallization of hBChE and Generation of CBDP-hBChE Conjugates. hBChE was concentrated to 9 mg/mL and crystallized using the hanging drop vapor-diffusion method as described previously.[19] Two different conjugates were obtained by soaking native crystals for either 2 min or 12 h at 4 °C in a mother liquor solution (0.1 M MES at pH 6.5 and 2.1 M ammonium sulfate) containing 1 mM CBDP. Crystals were then soaked for a few seconds in a cryoprotectant solution (0.1 M MES buffer at pH 6.5, 2.3 M ammonium sulfate, and 20% glycerol) before being flash-cooled in liquid nitrogen for data collection.

Crystallization of mAChE and Generation of CBDP-mAChE Conjugates. mAChE, concentrated to 14 mg/mL, was crystallized using the hanging drop vapor-diffusion method as described previously.[21] Two different conjugates were obtained by soaking native mAChE crystals for either 30 min or 12 h at 4 °C in a mother

dx.doi.org/10.1021/tx3004505 | *Chem. Res. Toxicol.* 2013, 26, 280−289

liquor solution (0.1 M Tris HCl buffer at pH 7.4 and 1.6 M ammonium sulfate) containing 1 mM CBDP. Crystals were soaked for a few seconds in a cryoprotective solution (0.1 M Tris HCl buffer at pH 7.4, 1.8 M ammonium sulfate, and 18% glycerol) and flash-cooled in liquid nitrogen.

X-ray Data Collection and Processing, Structure Determination, and Refinement. Diffraction data were collected on the ID14-eh4 beamline[22] at the European Synchrotron Radiation Facility (ESRF, Grenoble, France) with an ADSC Quantum Q315r detector. The beam was characterized by a wavelength of 0.9765 Å, and the crystals were held at 100 K during data collection. All data sets were processed with XDS,[23] intensities of integrated reflections were scaled using XSCALE, and structure factors were calculated using XDSCONV. The structures were solved by molecular replacement with the program MOLREP[24] of the CCP4 suite[25] using the recombinant hBChE structure (PDB entry 1P0I) and mAChE (PDB entry 4A16) as starting models. For all diffraction data sets, the initial models were refined as follows: a rigid-body refinement, carried out with REFMAC5,[26] was followed by iterative cycles of model building with Coot[27] and restrained TLS refinement was carried out with Phenix.[28] The bound ligands and their descriptions were built using the Dundee PRODRG2.5 server including energy minimization using GROMOS96.1 force field calculations. Successive alternation of refinement cycles and manual model building were performed until R_{cryst} and R_{free} did not decrease any further.

In addition, for mAChE, a refinement strategy involving TLS, Ramachandran, secondary structure restraints, and occupancy optimization was performed using Phenix. In the course of the refinement of oCSP-mAChE, it appeared that Phe297 adopts two alternative conformations and that occupancies of saligenin of oCSP-mAChE were partial. Therefore, the occupancies of Phe297 and saligenin in oCSP-mAChE were refined with Phenix as follows: *B*-factors and occupancy of Phe297 and saligenin were initially set to 30 Å^2 and 0.5, respectively. Then, coordinates and *B*-factors were refined resulting in a *B*-factor about 50 Å^2 for Ser198. To account for the higher disorder of oCSP, its *B*-factor was manually adjusted to the *B*-factor of Ser198 plus 20% (60 Å^2). Next, occupancies were refined, grouping the alternative conformation of Phe297 with saligenin. The resulting occupancies were rounded to the next digit, and a final refinement cycle of coordinate and *B*-factor was performed. Protein structures were illustrated using the program PyMOL (Schrödinger, LLC).

Mass Spectrometry of CBDP-mAChE and CBDP-hBChE after Reaction in $H_2{}^{18}O$. mAChE or hBChE (3.2 μM) was irreversibly inhibited by reaction with CBDP (93 μM) either in $H_2{}^{18}O$ (93% enriched) or $H_2{}^{16}O$ and 10 mM ammonium bicarbonate (pH 8) at 22 °C for 1 or 40 h. At the end of the inhibition period, there was no activity remaining for either mAChE or hBChE. Before proteolysis, water from both the $H_2{}^{18}O$ and $H_2{}^{16}O$ samples was removed by evaporation in a Savant SpeedVac (Thermo Fisher Scientific, Waltham, MA). The samples were then redissolved in $H_2{}^{16}O$ to a final concentration of 3.2 μM. Removal of the ^{18}O water simplified the mass spectra by preventing ^{18}O atoms from being incorporated into the carboxyl termini of the peptides during proteolysis. Proteolysis was performed by adding pepsin (5 mg/mL in 5% formic acid) to each tube to obtain a final cholinesterase to pepsin ratio of 1:2 (w/w) and a final pH of 2.5. Mixtures were incubated at 37 °C for 2 h. Aliquots of each digest were diluted 1 to 10 in 50% acetonitrile and 0.3% trifluoroacetic acid (TFA), spotted directly onto MALDI sample plates, and air-dried. Dried spots were overlaid with a 2,5-dihydroxy benzoic acid matrix (Acros Organics a part of the Thermo Fisher Scientific group, Geel, Belgium). Samples were analyzed in a MALDI TOF/TOF 4800 mass spectrometer (Applied Biosystems, Foster City, CA) in negative reflector mode with delayed extraction (625 ns) and a laser intensity of 5500 V.

Molecular Dynamics Simulations of oCP-mAChE. A monomer from the oCSP-mAChE X-ray structure was used as the initial model for molecular dynamics simulations. All crystallographic water molecules were conserved. Both alternate conformations of Phe297 being present in the experimental structure, we retained only the non-native one. The saligenin group located in the acyl-binding pocket was manually removed from the initial model in order to generate the oCP-mAChE conjugate. We developed a full force field (FF) for the o-CP serine. The modified serine was built using Chimera[29] with geometry optimization at the Molecular Mechanics level. RESP charges of the modified residue were calculated using the REDS server[30] following the recommended procedure, including a Quantum Mechanics optimization of the fragments achieved with the Gaussian09 package at the HF/6-31G* theoretical level. The new FF was included in the amber99sb FF.[31] When parameters (bond distances, angles, and dihedral) were not available in amber99sb, they were assigned from the General Amber Force Field[32] using Antechamber.[33] Molecular dynamics simulations were carried out using the GROMACS 4.5.4 package.[34] The protein system was immersed in a 10-Å layer truncated cubic periodic water box using the TIP3P solvation model.[35] Charge equilibration was made by adding 9 Na^+ ions. A 2-fs time step was used in all the simulations, and long-range electrostatic interactions were treated with the particle-mesh Ewald (PME) procedure[36] using a cubic B-spline interpolation and a 10^{-5} tolerance for the direct-space and with a 12-Å nonbonded cutoff. A 300 K temperature coupling scheme using a separated Berendsen thermostat for solvent and protein was applied. Pressure was kept constant at 1 bar by a Berendsen barostat considering a compressibility of 4.5×10^{-5}. Molecular dynamics was preceded by an energy minimization (500 cycles of Steepest Descent) and a 50 ps position-restrained MD-simulated soak. Six full MD simulations differing only by the seed used to generate initial velocities were performed for 10 ns at 300 K under these conditions. The resulting trajectories were visualized using VMD[37] and analyzed using the tools provided in the GROMACS package.

RESULTS

Crystallographic Structures of *o*-Cresyl-phospho-hBChE (oCP-hBChE) and Phospho-hBChE. The oCP-hBChE adduct was generated by soaking a hBChE crystal for 2 min in a mother liquor solution containing 1 mM CBDP. The crystal was then flash-cooled to 100 K, and diffraction data were collected to a resolution of 2.7 Å (Table 1).

The initial Fourier-difference electron density map ($F_o - F_c$) featured a strong positive peak (10.4 σ) at covalent bonding distance from catalytic Ser198Oγ (not shown), allowing to assign the position of the phosphorus atom of the CBDP adduct. The saligenin substituent was not present despite the short soaking time. Rather, the ligand was modeled as an *o*-cresyl phosphate, with its *o*-cresyl moiety bound in the acyl-binding pocket (Figure 1A); this binding scenario implies that the P(R) enantiomer of CBDP initially bound to the enzyme. In the refined model, the covalent bonds oCP600P-Ser198Oγ, Ser198Oγ-Ser198Cβ, and Ser198Cβ-Ser198Cα are elongated and characterized by distances of 2.0, 1.7, and 1.65 Å, respectively. These values can be compared to predicted values of 1.60, 1.45, and 1.55 Å (calculated *ab initio* using Gaussian09) and to observed values of 1.85, 1.45, and 1.55 Å, in the previously determined crystal structure of phospho-hBChE, the end product of the hBChE inhibition by CBDP (Figure 1B; pdb ID 2y1k). Restraining the length of these bonds to their ideal values led to the appearance, in the resulting Fourier-difference map, of a large negative peak (>5 σ) between the phosphorus atom and Ser198Oγ, and of equivalent positive peaks on the opposite side of the phosphorus atom and Ser198Oγ. We interpret this observation as an indication of strain in the 3 consecutive bonds between the phosphorus atom and the serine main chain, which we propose to stem from the steric exclusion of the *o*-cresyl group by Trp231 (closest distance between non-hydrogen atoms: 3.5 Å). The entire phosphoryl group is pushed-up the active site gorge by 1.3 Å

dx.doi.org/10.1021/tx3004505 | Chem. Res. Toxicol. 2013, 26, 280−289

Table 1. Crystallographic and Refinement Statistics

	oCP-BChE	oCSP-AChE	oCP-AChE
PDB entry code	4bbz	4bc0	4bc1
space group	*I*422	$P2_12_12_1$	$P2_12_12_1$
unit cell (Å)			
a	154.7	135.5	136.9
b	154.7	173.3	174.0
c	127.0	224.9	225.6
resolution (Å)	54.7−2.7	48.3−2.95	48.6−3.35
completeness (%)[a]	98.1 (99.0)	99.7 (99.4)	96.6 (98.6)
R_{sym} (%)[a]	7.1 (46.5)	8.1 (52.8)	7.5 (58.4)
$I/\sigma(I)$[a]	28.1 (5.2)	17.1 (3.1)	16.2 (2.8)
unique reflections[a]	21 049	111 473	75 488
redundancy[a]	10.1 (9.2)	4.4 (4.5)	3.6 (3.4)
Wilson *B* factor (Å^2)	53.4	63.9	94.92
R_{fact} (%)	16.6	18.6	16.2
R_{free} (%)	22.5	23.8	20.7
non-hydrogen atoms	4547	17994	17432
protein	4222	16 899	16 806
ligands	186	260	215
solvent	139	835	411
RMS bond length (Å)	0.008	0.009	0.009
RMS bond angles (deg)	1.269	1.368	1.482
Ramachandran			
favored (%)	94	92	94
allowed (%)	6	7.8	5.7
outliers (%)	0	1.2	0.3
average *B* factor (Å^2)	41.3	46.8	47.2
protein	40	46.9	47.1
ligands	74.1	91.2	92.7
solvent	36.2	31.5	28.3

[a]Values in parentheses refer to the highest resolution shell.

and twisted counter-clockwise around the Ser198Oγ-P bond when compared to its conformation in the phospho-BChE structure (Figure 2, panel A). This results in the absence of hydrogen-bonding interaction between the phosphoryl oxygen (O3P) of oCP600 and Ala199N in the oxyanion hole, again in contrast to what is observed in the phospho-hBChE structure (4.5 Å interatomic distance vs 2.7 Å in the oCP- and phospho-hBChE structures, respectively). Likewise, the hydrogen bond interaction between O1P of oCP and His438Nε2 and Ser198Oγ are both weakened (3.3 Å and 3.2 Å, respectively) relative to phospho-hBChE (2.9 Å and 3.0 Å; Figure 1B).

Altogether, these observations indicate that the oCP-hBChE adduct is not as stable as a canonical aged-BChE-OP conjugate, which the phospho-hBChE structure resembles more.

Crystallographic Structure of *o*-Cresyl Saligenin Phospho-mAChE (oCSP-mAChE). The oCSP-mAChE adduct was trapped by flash cooling a mAChE crystal that had been soaked for 30 min in a mother liquor solution containing 1 mM CBDP. The structure was solved at 2.95 Å resolution (Table 1). In this space group, the asymmetric unit contains two mAChE biological dimers that are related by noncrystallographic symmetry, and in each, monomers associate through a four helix-bundle.[38] In each dimer, one monomer features a solvent accessible peripheral site, while the peripheral site of the other is occupied by the Cys257-Cys272 loop from another monomer in the asymmetric unit tetramer. The *o*-cresyl and saligenin substituents are located in the choline- and acyl-binding pockets, respectively, indicating a preferential binding of the P(S) enantiomer of CBDP in mAChE (Figure 1C). This is in contrast with hBChE, in which it is the P(R) enantiomer that preferentially binds and where the *o*-cresyl substituent is located in the acyl-binding pocket (Figure 1A). In the acyl-binding pocket of oCSP-mAChE, Phe297 adopts an alternate conformation with a χ1 rotation of about 145° (around the Cα-Cβ bond), as required for the accommodation of saligenin (Figure 1C). We used the direct correlation between the alternate conformation of Phe297 and the presence of the saligenin moiety in the acyl-binding site to evaluate the partial occupancy of saligenin in the oCSP-mAChE structure (see the Experimental Procedures section for details). The fraction of bound CBDP retaining saligenin ranges from 0.4 to 0.5, depending on which of the four monomers is inspected. Overall, the geometry of catalytic-Ser203 in oCSP-mAChE is not distorted compared to catalytic-Ser198 in oCP-hBChE (Figure 2, compare the slate colored structures in panels A and B). The refined length of the covalent oCSP600P-Ser203Oγ bond is 1.7 Å in the mAChE structure, compared to a predicted value of 1.59 Å (as calculated *ab initio*). Finally, the catalytic His447Nε2 forms a H-bond with Ser203Oγ (2.8 Å) but does not interact with O2P of the cresyl substituent (Figure 1C).

Crystallographic Structure of *o*-Cresyl-phospho-mAChE (oCP-mAChE). The oCP-mAChE adduct was obtained by extending the soaking time to 12 h before flash cooling the crystal. The resolution of this structure is relatively low (3.35 Å) in comparison to that of the analogous oCP-hBChE structure (Table 1). It is unclear whether it is the relatively long soaking time or the effect of enzymatically produced saligenin that affected the crystal quality and the resolution of the diffraction data. Electron density maps were yet of good quality and thus allowed the unambiguous modeling of the *o*-cresyl moiety into a strong peak of positive $F_o - F_c$ electron density (10 σ) in the vicinity of the catalytic-serine hydroxyl group (Figure 1D). No electron density is observed in the acyl-binding pocket, indicating that the saligenin moiety has exited the active site (Figure 1D). Accordingly, Phe297 fully occupies its native position as indicated by the electron density maps and further confirmed by the occupancy refinement of its side chain. The *o*-cresyl moiety is stabilized in the choline-binding pocket by a perpendicular π-stacking interaction with the aromatic rings of Trp86. No H-bond interaction is noticeable between the *o*-cresyl O2 atom and His447Nε2, the later being hydrogen-bonded to Ser203Oγ (2.9 Å). With the *o*-cresyl substituent in the choline-binding pocket, the oCP-mAChE adduct appears to be the mirror image of the oCP-hBChE adduct in which the substituent is found in the acyl-binding pocket (Figure 1A and D). X-ray data collected after soaking periods ≥12 h repeatedly yielded an oCP-mAChE adduct and not a phosphoserine adduct as observed in hBChE.

Mass Spectrometry Analysis. The repeatedly unproductive attempts to obtain the structure of a phospho-mAChE adduct suggested that CBDP inhibition of mAChE occurs in two steps, i.e. phosphorylation of the enzyme and a canonical aging reaction. From our crystallographic data alone, however, we could not determine whether the observation of an *o*-cresyl phosphoserine adduct as the end-product of mAChE inhibition by CBDP was a crystallographic artifact or, rather, a sign for CBDP inhibition of AChE and BChE occurring through different pathways.

In order to ascertain the number of steps involved in the *in vitro* mAChE inhibition by CBDP, MALDI-TOF mass-spectrometry of proteolyzed, CBDP-inhibited mAChE was

dx.doi.org/10.1021/tx3004505 | *Chem. Res. Toxicol.* 2013, 26, 280−289

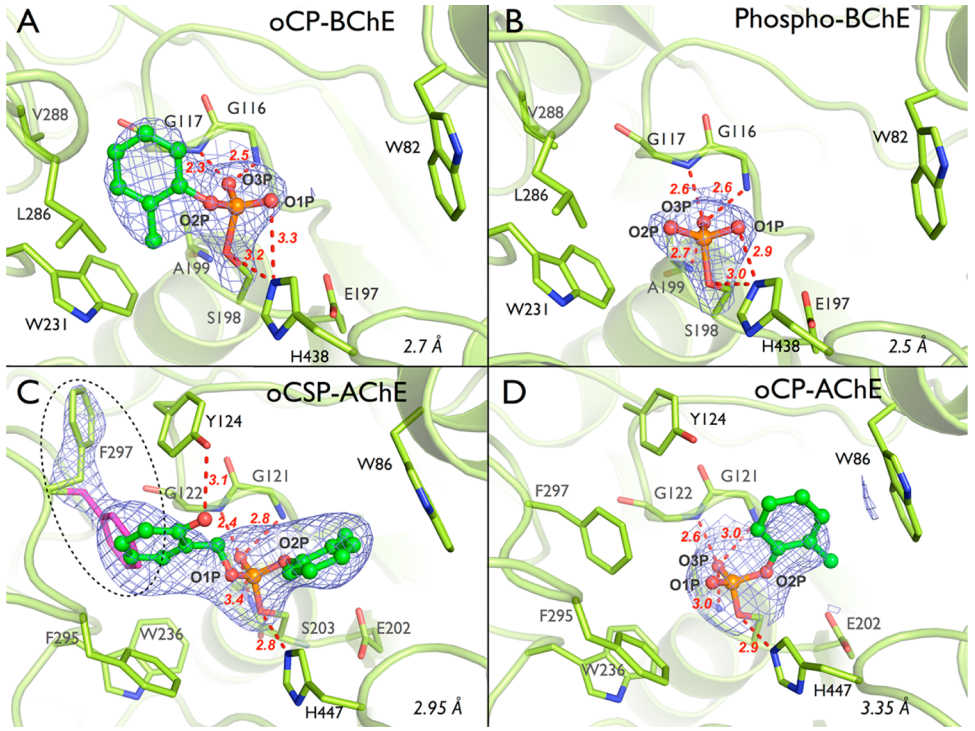

Figure 1. Sequential crystallographic snapshots of mAChE and BChE inhibition by CBDP. For BChE (upper panels), a soaking time of 2 min yielded an *o*-cresyl-phospho-BChE conjugate (A, current work). A soaking time of 12 h yielded the final phospho-BChE conjugate[7] (B). For mAChE (lower panels), soaking times of 30 min and 12 h yielded the *o*-cresyl saligenin phospho-AChE conjugate (C) and the *o*-cresyl-phospho-AChE conjugate (D), respectively. Key residues are represented as sticks with carbon atoms in green, nitrogen atoms in blue, phosphorus in orange, and oxygen atoms in red. Atoms and bonds of the adducts are represented as ball and sticks, respectively. Hydrogen bonds are represented by red dashes with distances in Å. A dashed ellipse in panel C highlights the native (magenta) and an alternate (green) position of Phe297. The electron density $2F_o - F_c$ is represented by a blue mesh contoured at 1.0 σ.

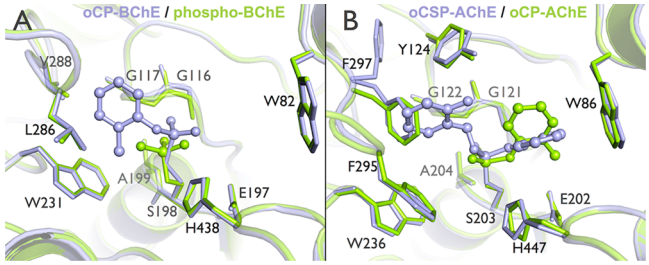

Figure 2. (A) Superimposition of oCP-BChE (slate) and phospho-BChE (green) structures. (B) Superimposition of oCSP-AChE (slate) and oCP-AChE (green) structures. Key residues are represented as sticks. Atoms and bonds of the adducts are represented as ball and sticks, respectively.

used, as previously described for hBChE.[7] We investigated the involvement of water molecules in the various steps of mAChE inhibition by CBDP by performing the inhibition in either $H_2{}^{16}O$ or in $H_2{}^{18}O$, which allowed us to characterize the step at which water is incorporated into the enzyme adducts. As a control, the same analyses were performed on CBDP-inhibited hBChE. Inhibition yields reached 100%, for both mAChE and hBChE, as evidenced by the absence of catalytic activity at the end of the reaction period and by the absence of unlabeled active-site peptides in the mass spectra.

From the hBChE-CBDP reaction, both *o*-cresyl phosphate (oCP) and phosphate adducts on the active-site peptic-peptide were detected.[18] Post source decay fragmentation confirmed that these adducts were on the active-site serine. Figure 3, panels A and B, show mass spectra (in negative mode) for *o*-cresyl phosphate adducts at 877 amu (for the peptic peptide FGESAGAA) and at 964 amu (for the miscleavage peptide FGESAGAAS). These adducts are formed following the release of saligenin from the initial CBDP-hBChE reaction product. The masses of these adducts are not affected by the presence of $H_2{}^{18}O$ indicating that no oxygen atoms from water are incorporated into the phosphorus moiety upon the release of saligenin. Figure 3, panels A and B, also show mass spectra (negative mode) for phosphate adducts. In $H_2{}^{16}O$, the phosphate adduct appears at 874 amu (for peptide FGESAGAAS). In $H_2{}^{18}O$, the 874 amu mass is shifted to 876 amu indicating the incorporation of an oxygen atom from water into the phosphate adduct upon the hydrolytic release of the *o*-cresyl moiety.

From the mAChE-CBDP reaction, only an *o*-cresyl-phosphate adduct was detected (Figure 3, panels C–D). No evidence for the phosphate adduct was obtained after the 1 h reaction period used for this experiment, nor was the phosphate adduct detected when the reaction was allowed to proceed for 40 h. Post-source decay fragmentation showed that the *o*-cresyl phosphate adduct was located on the active site serine. In mass spectra (negative mode) for both the $H_2{}^{16}O$ and $H_2{}^{18}O$ samples, masses for the oCP adducts appeared at 877 amu (for peptide FGESAGAA) and 964 amu (for peptide FGESAGAAS) indicating that no oxygen atom from water is incorporated into the adduct upon release of saligenin.

Molecular Dynamics Simulations. Phe297 is in an alternate conformation in the oCSP-mAChE adduct and moved back to its native position during aging as seen in the crystallographic structure of the oCP-mAChE adduct. We

dx.doi.org/10.1021/tx3004505 | *Chem. Res. Toxicol.* 2013, 26, 280–289

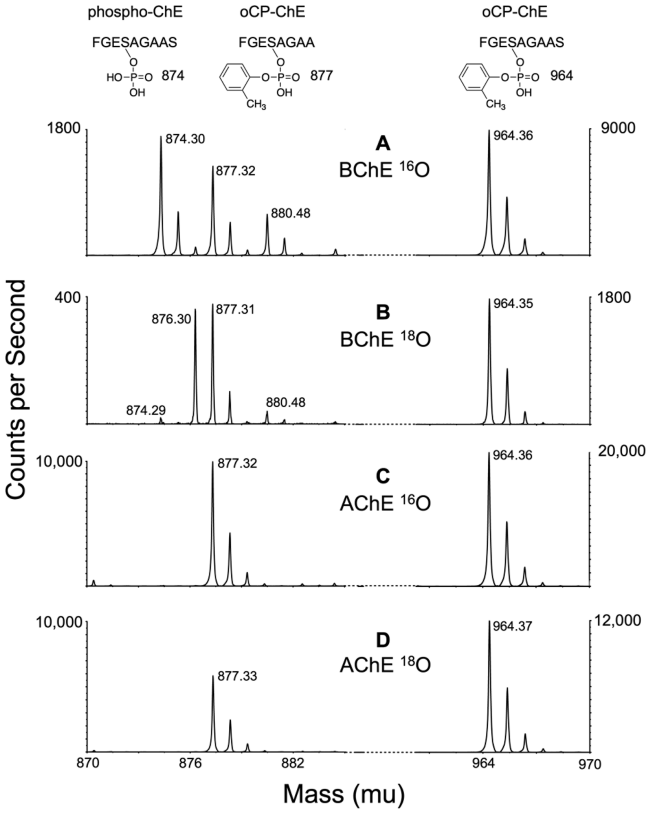

Figure 3. Reaction of hBChE and mAChE with CBDP in the presence of O^{16}-water (A and C) and O^{18}-water (B and D). The 874−877 amu region and 964 amu region of pepsin-digested 1-h CBDP-inhibited ChEs are shown. All spectra were taken in negative mode. The sequence of the phosphopeptide of mass 874 is FGES*AGAAS with PO_4 on serine. The sequences of the *o*-cresyl phosphate adducts of mass 877 and 964 are FGES*AGAA and FGES*AGAAS, where the asterisk indicates the labeled serine.

carried out molecular dynamics (MD) simulations in order to address whether the observed conformational change is part of equilibrium dynamics preexisting to ligand binding or a fit induced by ligand binding.[39] An initial model was created based on the oCSP-mAChE crystallographic structure, i.e., with the side chain of Phe297 in the alternate conformation but not with the saligenin substituent. In none of the six 10-ns MD simulations was a reversal of Phe297 to its native conformation observed.

DISCUSSION

Previously, we showed that hBChE inhibition by CBDP proceeds through a three-step reaction mechanism.[18] First, the catalytic serine is organophosphorylated to form the ring-opened CBDP-hBChE adduct. A dealkylation step then occurs viz. the first aging reaction, which results in the loss of the saligenin moiety. Last, the oCP-hBChE adduct undergoes hydrolysis with the concomitant departure of the *o*-cresyl moiety yielding the final phosphoserine hBChE adduct (Scheme 1).[7] That the latter is the end product of hBChE inhibition by CBDP was known from its X-ray structure at 2.7 Å resolution as well as from previous mass spectrometry experiments. It remained unclear, however, how these steps proceed at the atomic level of resolution. Also, it was unknown if mAChE follows the same inhibition pathway as hBChE and/or displays the same enantiomer selectivity.

In the current study, a combination of X-ray crystallography and mass-spectrometry was used to specifically address the above-mentioned unresolved issues. Atomic-resolution crystallographic snapshots of hBChE and mAChE were taken at different time points during their reaction with CBDP. Together with adduct masses obtained from the mass spectra, they allow one to develop detailed mechanistic models for the CBDP inhibitions of mAChE and hBChE, respectively.

Inhibition of mAChE by CBDP. In this study, mAChE was employed instead of hAChE because our preparation of the latter only crystallizes in the presence of the gorge-capping peptide fasciculin. Such capping prevents inhibitors from entering the active site precluding the use of soaking techniques to introduce inhibitors. mAChE is yet a reliable model for hAChE in that nearly all of the residues lining the active site gorge of mAChE and hAChE are identical. Noteworthy, Cheung et al. very recently reported a truncated form of hAChE able to crystallize without fasciculin and suitable for soaking techniques.[40] Use of this new form of hAChE will be preferred for future crystallographic studies.

After soaking a crystal of mAChE for 30 min in a CBDP containing solution, the initial ring-opened oCSP-AChE adduct could be trapped by flash cooling (Figure 1C). The *o*-cresyl and saligenin moieties are located in the choline- and the acyl-binding pockets, respectively. This positioning indicates that crystalline mAChE preferentially binds and reacts with the P(S) enantiomer of CBDP.

Figure 1C also shows that the acyl-binding pocket is only partially occupied by saligenin. The partial occupancy (0.4−0.5) indicates that about half of the crystalline oCSP adducts have released saligenin after a 30 min soak (note that the *o*-cresyl site is fully occupied). Thus, the half-life for the first aging reaction is about 30 min *in crystallo*. Extending the soaking time to 12 h or more results in the complete elimination of saligenin and in the formation of an oCP-AChE conjugate (Figure 1D).

Mass spectral analysis after proteolysis, combined with the crystal structures, shows that mAChE inhibition by CBDP occurs in two steps, viz. organophosphorylation and dealkylation of saligenin in the acyl-binding pocket, yielding a final *o*-cresyl-phosphoserine adduct (Scheme 2). The fact that no water was incorporated in the *o*-cresyl-phosphoserine mAChE adduct indeed excludes the possibility that saligenin was released through its hydrolysis. Dealkylation is an unusual reaction for a substituent located in the acyl-binding pocket: the two residues known to catalyze dealkylation of OPs adducts, His447 and Glu202, are indeed part of the choline-binding pocket, on the opposite site of the active site gorge. No unusual strain is observed in the o-CSP adduct, which eliminates this source of enthalpy as the driving force for the dealkylation reaction. This implies that another driving force must be involved. A possibility is that the hydroxyl group of saligenin stabilizes a water molecule that could in turn react with the benzylic carbocation, thereby promoting the dealkylation reaction. The return to its native conformation of the Phe297 side chain, which was displaced from the acyl-binding pocket by the saligenin substituent, could constitute an additional driving force for the dealkylation.

Both the 40-h mass spectrometry and the 12-h crystallographic data indicate that the oCP adduct is the end product of mAChE inhibition by CBDP, in contrast to hBChE where the oCP adduct reacts further to yield a phosphoserine adduct (Figure 1B).[7] This difference is most likely to ascribe to the

dx.doi.org/10.1021/tx3004505 | *Chem. Res. Toxicol.* 2013, 26, 280−289

Scheme 2. Detailed Chemical Mechanism for CBDP Inhibition of mAChE and hBChE

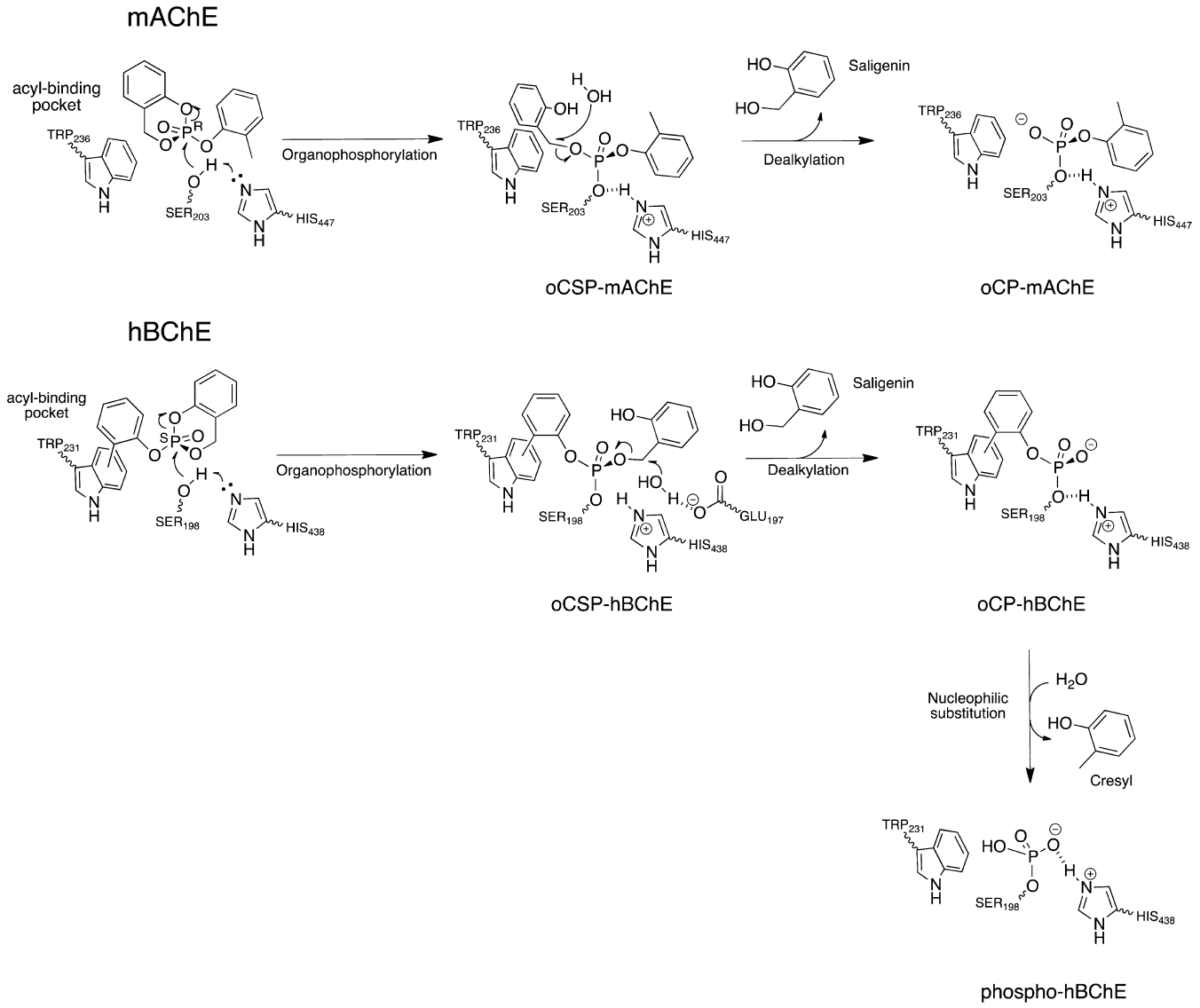

symmetric configuration of the *o*-cresyl substituent in mAChE and hBChE. In hBChE, the *o*-cresyl substituent is in the acyl-binding pocket; thus, the choline-binding pocket remains free for a water to approach the phosphorus atom, resulting in oCP adduct hydrolysis. Conversely in mAChE, hydrolysis does not occur because the *o*-cresyl substituent is located in the choline-binding pocket, meaning that the water would have to attack from the crowded acyl-binding pocket. While dearylation of the oCP-mAChE adduct could theoretically have occurred, considering that the *o*-cresyl substituent is located in proximity to His447/Glu202, our data unequivocally show that it does not. In this context, it is noteworthy mentioning that one of the strategies envisaged to counteract OP-intoxication is to realkykate aged phosphylconjugates;[41] by showing that dearylation does not occur on the time scale of our experiments (tens of hours), our data thus suggest that arylation may be more promising than realkylation.

In mAChE, organophosphorylation correlates with a rotation of the Phe297 side chain (Figure 1C), which enlarges the acyl-binding pocket and is thus required to accommodate the saligenin moiety. An identical conformational change was observed in the crystal structures of fenamiphos-inhibited mAChE in complex with the ortho-7 reactivator (pdb accession code 2wu4)[42] as well as in a *Tc*AChE/Bis(5)-tacrine complex (pdb accession code 2cmf).[43] In the ortho-7 complex, one pyridinium ring of ortho-7 pushes the isopropylamino substituent of fenamiphos toward the acyl-loop 285−298 and leads to its rearrangement. In the *Tc*AChE complex, non-covalent binding of the tacrine produces drastic rearrangements in the active site gorge, including a rotation of Phe290 (Phe297 in mAChE), that are induced by a tilt of Tyr121.[43] Since molecular dynamics simulations of native *Tc*AChE did not reveal alternate Phe290 conformations,[44] the rotation seen in the *Tc*AChE/Bis(5)-tacrine complex must be induced by the ligand rather than being selected by the ligand among preexisting native conformations. By extrapolation, the rotation of Phe297 observed in mAChE is also most likely the consequence of an induced fit mechanism, meaning that the conformational change is induced by ligand binding, rather than being part of preexisting equilibrium fluctuations. Although the acyl-loop determines the specificity of hAChE for the natural substrate acetylcholine,[45,46] the acyl-loop remains flexible enough to accommodate bulkier ligands at the cost of an induced fit rearrangement. This rearrangement is reversed once

dx.doi.org/10.1021/tx3004505 | *Chem. Res. Toxicol.* 2013, 26, 280−289

the acyl-binding pocket becomes unoccupied, as after the aging of oCSP-mAChE. The conformational change was not reproduced in six 10 ns molecular dynamics simulations, indicating that the crystallographically observed conformational change is not a simple side chain flip but rather requires a larger rearrangement of the acyl-loop region that is not observed on the time scale of the simulations. These larger rearrangements of the acyl-loop are probably part of the proposed induced-fit mechanism.

Inhibition of hBChE by CBDP. The first species observed in the reaction of CBDP with hBChE is oCP-hBChE (Figure 1A), which corresponds to the second intermediate in the reaction mechanism (see Scheme 1). oCP-hBChE is created by the loss of saligenin from the initial intermediate, the ring-opened CBDP adduct. The latter could not be trapped, even by reducing soaking times to as short as 30 s, indicating that this adduct decays faster than it forms.

The *o*-cresyl moiety is located in the acyl-binding pocket of the oCP-hBChE adduct, which indicates that the saligenin moiety was bound in the choline-binding pocket prior to the first aging step and suggests a preferential reaction of the P(R) enantiomer of CBDP with crystalline hBChE. MD and QM/MM studies of hBChE reacting with CBDP, as well as titration experiments, support the proposed stereoselectivity (Lushchekina et al., unpublished results). Mass spectrometry showed that no oxygen atom from water is incorporated into the oCP-adduct, inferring that the release of saligenin likely stems from a His438/Glu197-catalyzed dealkylation.[7] This conclusion is in agreement with the proposal that aging of OP-hBChE proceeds through O-dealkylation of substituents bound in the choline-binding pocket.[47] However, an oxygen atom from water is incorporated during the second aging reaction. This observation supports the hypothesis of a nucleophilic attack, by a water molecule, on the phosphorus atom of oCP, resulting in the release of the o-cresyl moiety and the formation of the phospho-BChE adduct.[7]

From a mechanistic point of view, the most probable scenario is that this water attacks from the open face opposite the cresyl−O-P bond, vicinal to Glu197 (refer to Figure 1A), leading to the formation of a bipyramidal transition state and its subsequent collapse, with the release of *o*-cresyl (Scheme 2). The other possibility is that water approaches from the side opposite to the Ser198Oγ-P bond. However, we conjecture this scenario is unlikely considering the steric hindrance imposed by the presence of the *o*-cresyl moiety in the acyl-binding pocket. Also, a water attack from that side should lead to the scission of the Ser198Oγ-P bond and, therefore, to the release of the entire *o*-cresyl phosphate group, not just the *o*-cresyl moiety. Yet, neither was a native active site peptide identified in our mass spectrometry study, nor was self-reactivation observed in our previous kinetics studies. Thus, the attack of water is proposed to occur from the open face opposite the cresyl−O-P bond, vicinal to Glu197. A similar mechanism was proposed for the aging reaction of an analogue of the nerve agent tabun.[48]

A structural comparison between the oCP- and the phospho-hBChE adducts shows a release of the strain imposed on the enzyme, when *o*-cresyl is released and the phospho-conjugate is formed (Figures 2A). We conjecture that the release of this strain contributes to the driving force responsible for the scission of the P−O bond linking the *o*-cresyl to the phosphorus. It should be noted that unlike in mAChE, no side chain undergoes major conformational changes upon the binding of CBDP in hBChE.

CONCLUSIONS

The combination of crystallographic snapshots with mass spectrometric analysis shows that the inhibition of mAChE and hBChE by CBDP involves the binding of opposite enantiomers. Therefore, two different reaction pathways are undertaken by mAChE and hBChE for inhibition and aging. hBChE undergoes a three-step reaction process including (i) the organophosphorylation of the catalytic serine to form a CBDP ring-opened adduct, (ii) a dealkylation resulting in the loss of the saligenin substituent from the choline-binding pocket, and (iii) a nucleophilic hydrolysis of the *o*-cresyl substituent in the acyl-binding pocket, yielding a final phosphoserine-hBChE conjugate. In contrast, the inhibition of mAChE is a two-step reaction, resulting from of organophosphorylation and subsequent dealkylation, leading to the release of saligenin and the formation of the *o*-cresyl-phosphoserine mAChE adduct. Additionally, the crystallographic snapshots of the mAChE inhibition intermediates illustrate how a bulky inhibitor like CBDP is able to fit into the active site of mAChE through an induced fit rearrangement. It is worth noting that for both mAChE and hBChE, the final enzyme conjugate is aged, meaning that it cannot be reactivated by oximes.[47] In other words, there is currently no effective therapeutics to reactivate inhibited AChE in the case of severe TOCP intoxication.

ASSOCIATED CONTENT

Supporting Information

$2F_o - F_c$ and $F_o - F_c$ electron density maps. This material is available free of charge via the Internet at http://pubs.acs.org.

AUTHOR INFORMATION

Corresponding Author

*(F.N.) Tel: (+33) 476 636959. E-mail: florian@nachon.net. (M.W.) Tel: (+33) 438 789580. E-mail: martin.weik@ibs.fr.

Funding

Financial support by the DGA (project number DGA-REI 2009-34-0023 to M.W. and DGA/DSP/STTC 08co501 to F.N.), CEA, the CNRS, and the UJF is acknowledged, as well as grants from the Agence Nationale de la Recherche (ANR; project number ANR-09-BLAN-0192-04 to M.W. and F.N.) and the DTRA (HDTRA1-11-C-0047 to M.W. and F.N.). J.P.C. is a recipient of the Young International Scientists fellowship from the Chinese Academy of Science.

Notes

The authors declare no competing financial interest.

ACKNOWLEDGMENTS

We are grateful to the ESRF for beam-time under long-term projects MX498, MX609, and MX722 (IBS BAG), and MX551 and MX 666 (radiation-damage BAG), and to the ESRF staff for providing efficient help during data collection. Mass spectra were obtained with the support of the Mass Spectrometry and Proteomics core facility at the University of Nebraska Medical Center.

ABBREVIATIONS

TOCP, tri-*o*-cresyl-phosphate; TCP, tricresyl phosphate; CBDP, 2-(*ortho*-cresyl)-4*H*-1,2,3-benzodioxaphosphoran-2-one, cresyl saligenin phosphate; OP, organophosphorus compound; hBChE, human butyrylcholinesterase; hAChE, human acetylcholinesterase; mAChE, mouse acetylcholinester-

ase; ChE, cholinesterase; oCP-hBChE, *o*-cresyl phosphate human butyrylcholinesterase conjugate; oCP, *o*-cresyl phosphate; oCSP-mAChE, *o*-cresyl saligenin phosphate mouse acetylcholinesterase conjugate; oCSP, *o*-cresyl saligenin phosphate; oCP-mAChE, *o*-cresyl phosphate mouse acetylcholinesterase conjugate

REFERENCES

(1) Winder, C. (2006) Air monitoring studies for aircraft cabin contamination. *Curr. Top. Toxicol. 3*, 33−48.

(2) Mackerer, C. R., Barth, M. L., Krueger, A. J., Chawla, B., and Roy, T. A. (1999) Comparison of neurotoxic effects and potential risks from oral administration or ingestion of tricresyl phosphate and jet engine oil containing tricresyl phosphate. *J. Toxicol. Environ. Health, Part A 57*, 293−328.

(3) Liyasova, M., Li, B., Schopfer, L. M., Nachon, F., Masson, P., Furlong, C. E., and Lockridge, O. (2011) Exposure to tri-o-cresyl phosphate detected in jet airplane passengers. *Toxicol. Appl. Pharmacol. 256*, 337−347.

(4) Casida, J. E., Eto, M., and Baron, R. L. (1961) Biological activity of a trio-cresyl phosphate metabolite. *Nature 191*, 1396−1397.

(5) Eto, M., Casida, J. E., and Eto, T. (1962) Hydroxylation and cyclization reactions involved in the metabolism of tri-o-cresyl phosphate. *Biochem. Pharmacol. 11*, 337−352.

(6) Eto, M., Oshima, Y., and Casida, J. E. (1967) Plasma albumin as a catalyst in cyclization of diaryl o-(alpha-hydroxy)tolyl phosphates. *Biochem. Pharmacol. 16*, 295−308.

(7) Carletti, E., Schopfer, L. M., Colletier, J. P., Froment, M. T., Nachon, F., Weik, M., Lockridge, O., and Masson, P. (2011) Reaction of cresyl saligenin phosphate, the organophosphorus agent implicated in aerotoxic syndrome, with human cholinesterases: mechanistic studies employing kinetics, mass spectrometry, and X-ray structure analysis. *Chem. Res. Toxicol. 24*, 797−808.

(8) Masson, P. (2011) Evolution of and perspectives on therapeutic approaches to nerve agent poisoning. *Toxicol. Lett. 206*, 5−13.

(9) Worek, F., Thiermann, H., Szinicz, L., and Eyer, P. (2004) Kinetic analysis of interactions between human acetylcholinesterase, structurally different organophosphorus compounds and oximes. *Biochem. Pharmacol. 68*, 2237−2248.

(10) Harel, M., Schalk, I., Ehret-Sabatier, L., Bouet, F., Goeldner, M., Hirth, C., Axelsen, P. H., Silman, I., and Sussman, J. L. (1993) Quaternary ligand binding to aromatic residues in the active-site gorge of acetylcholinesterase. *Proc. Natl. Acad. Sci. U.S.A. 90*, 9031−9035.

(11) Wandhammer, M., Carletti, E., Van der Schans, M., Gillon, E., Nicolet, Y., Masson, P., Goeldner, M., Noort, D., and Nachon, F. (2011) Structural study of the complex stereoselectivity of human butyrylcholinesterase for the neurotoxic V-agents. *J. Biol. Chem. 286*, 16783−16789.

(12) Winder, C., and Balouet, J. C. (2002) The toxicity of commercial jet oils. *Environ. Res. 89*, 146−164.

(13) van Netten, C. (2005) Aircraft air quality incidents: symptoms, exposures and possible solutions. *J. Occup. Health Saf. 21*, 460−468.

(14) Johnson, M. K. (1975) Structure-activity relationships for substrates and inhibitors of hen brain neurotoxic esterase. *Biochem. Pharmacol. 24*, 797−805.

(15) Glynn, P. (1999) Neuropathy target esterase. *Biochem. J. 344*, 625−631.

(16) Aldridge, W. N. (1954) Tricresyl phosphates and cholinesterase. *Biochem. J. 56*, 185−189.

(17) Earl, C. J., and Thompson, R. H. (1952) The inhibitory action of tri-ortho-cresyl phosphate on cholinesterases. *Br. J. Pharmacol. Chemother. 7*, 261−269.

(18) Schopfer, L. M., Furlong, C. E., and Lockridge, O. (2010) Development of diagnostics in the search for an explanation of aerotoxic syndrome. *Anal. Biochem. 404*, 64−74.

(19) Nachon, F., Nicolet, Y., Viguie, N., Masson, P., Fontecilla-Camps, J. C., and Lockridge, O. (2002) Engineering of a monomeric and low-glycosylated form of human butyrylcholinesterase: expression, purification, characterization and crystallization. *Eur. J. Biochem. 269*, 630−637.

(20) Carletti, E., Li, H., Li, B., Ekstrom, F., Nicolet, Y., Loiodice, M., Gillon, E., Froment, M. T., Lockridge, O., Schopfer, L. M., Masson, P., and Nachon, F. (2008) Aging of cholinesterases phosphylated by tabun proceeds through O-dealkylation. *J. Am. Chem. Soc. 130*, 16011−16020.

(21) Ronco, C., Carletti, E., Colletier, J. P., Weik, M., Nachon, F., Jean, L., and Renard, P. Y. (2011) Huprine derivatives as subnanomolar human acetylcholinesterase inhibitors: from rational design to validation by X-ray crystallography. *ChemMedChem 6*, 876−888.

(22) McCarthy, A. A., Brockhauser, S., Nurizzo, D., Theveneau, P., Mairs, T., Spruce, D., Guijarro, M., Lesourd, M., Ravelli, R. B., and McSweeney, S. (2009) A decade of user operation on the macromolecular crystallography MAD beamline ID14−4 at the ESRF. *J. Synchrotron Radiat. 16*, 803−812.

(23) Kabsch, W. (2010) XDS. *Acta Crystallogr., Sect. D 66*, 125−132.

(24) Vagin, A., and Teplyakov, A. (1997) MOLREP: an automated program for molecular replacement. *J. Appl. Crystallogr. 30*, 1022−1025.

(25) Collaborative-Computational-Project-4 (1994) The CCP4 suite: programs for protein crystallography. *Acta Crystallogr., Sect. D 50*, 760−763.

(26) Murshudov, G. N., Vagin, A. A., and Dodson, E. J. (1997) Refinement of macromolecular structures by the maximum-likelihood method. *Acta Crystallogr., Sect. D 53*, 240−255.

(27) Emsley, P., Lohkamp, B., Scott, W. G., and Cowtan, K. (2010) Features and development of Coot. *Acta Crystallogr., Sect. D 66*, 486−501.

(28) Adams, P. D., Afonine, P. V., Bunkoczi, G., Chen, V. B., Davis, I. W., Echols, N., Headd, J. J., Hung, L. W., Kapral, G. J., Grosse-Kunstleve, R. W., McCoy, A. J., Moriarty, N. W., Oeffner, R., Read, R. J., Richardson, D. C., Richardson, J. S., Terwilliger, T. C., and Zwart, P. H. (2010) PHENIX: a comprehensive Python-based system for macromolecular structure solution. *Acta Crystallogr., Sect. D 66*, 213−221.

(29) Pettersen, E. F., Goddard, T. D., Huang, C. C., Couch, G. S., Greenblatt, D. M., Meng, E. C., and Ferrin, T. E. (2004) UCSF Chimera: a visualization system for exploratory research and analysis. *J. Comput. Chem. 25*, 1605−1612.

(30) Vanquelef, E., Simon, S., Marquant, G., Garcia, E., Klimerak, G., Delepine, J. C., Cieplak, P., and Dupradeau, F. Y. (2011) R.E.D. Server: a web service for deriving RESP and ESP charges and building force field libraries for new molecules and molecular fragments. *Nucleic Acids Res. 39*, W511−517.

(31) Hornak, V., Abel, R., Okur, A., Strockbine, B., Roitberg, A., and Simmerling, C. (2006) Comparison of multiple Amber force fields and development of improved protein backbone parameters. *Proteins 65*, 712−725.

(32) Wang, J., Wolf, R. M., Caldwell, J. W., Kollman, P. A., and Case, D. A. (2004) Development and testing of a general amber force field. *J. Comput. Chem. 25*, 1157−1174.

(33) Wang, J., Wang, W., Kollman, P. A., and Case, D. A. (2006) Automatic atom type and bond type perception in molecular mechanical calculations. *J. Mol. Graphics Modell. 25*, 247−260.

(34) Hess, B., Kutzner, C., van der Spoel, D., and Lindahl, E. (2008) GROMACS 4: algorithms for highly efficient, load-balanced, and scalable molecular simulation. *J. Chem. Theory Comput. 4*, 435−447.

(35) Mahoney, M., and Jorgensen, W. (2000) A five-site model for liquid water and the reproduction of the density anomaly by rigid, nonpolarizable potential functions. *J. Chem. Phys. 112*, 8910−8922.

(36) Darden, T., York, D., and Pedersen, L. (1993) Particle mesh Ewald: an N.Log(N) method for Ewald sums in large systems. *J. Chem. Phys. 98*, 10089−10092.

(37) Humphrey, W., Dalke, A., and Schulten, K. (1996) VMD: visual molecular dynamics. *J. Mol. Graphics 14*, 33−38.

(38) Bourne, Y., Taylor, P., Bougis, P. E., and Marchot, P. (1999) Crystal structure of mouse acetylcholinesterase. A peripheral site-

occluding loop in a tetrameric assembly. *J. Biol. Chem. 274*, 2963−2970.
(39) Xu, Y., Colletier, J. P., Jiang, H., Silman, I., Sussman, J. L., and Weik, M. (2008) Induced-fit or preexisting equilibrium dynamics? Lessons from protein crystallography and MD simulations on acetylcholinesterase and implications for structure-based drug design. *Protein Sci. 17*, 601−605.
(40) Cheung, J., Rudolph, M. J., Burshteyn, F., Cassidy, M. S., Gary, E. N., Love, J., Franklin, M. C., and Height, J. J. (2012) Structures of human acetylcholinesterase in complex with pharmacologically important ligands. *J. Med. Chem. 55*, 10282−10286.
(41) Wandhammer, M., de Koning, M., van Grol, M., Loiodice, M., Saurel, L., Noort, D., Goeldner, M., and Nachon, F. (2012) A step toward the reactivation of aged cholinesterases - Crystal structure of ligands binding to aged human butyrylcholinesterase. *Chem.-Biol. Interact.*, DOI: 10.1016/j.cbi.2012.1008.1005.
(42) Hornberg, A., Artursson, E., Warme, R., Pang, Y. P., and Ekstrom, F. (2010) Crystal structures of oxime-bound fenamiphos-acetylcholinesterases: reactivation involving flipping of the His447 ring to form a reactive Glu334-His447-oxime triad. *Biochem. Pharmacol. 79*, 507−515.
(43) Rydberg, E. H., Brumshtein, B., Greenblatt, H. M., Wong, D. M., Shaya, D., Williams, L. D., Carlier, P. R., Pang, Y. P., Silman, I., and Sussman, J. L. (2006) Complexes of alkylene-linked tacrine dimers with Torpedo californica acetylcholinesterase: Binding of Bis5-tacrine produces a dramatic rearrangement in the active-site gorge. *J. Med. Chem. 49*, 5491−5500.
(44) Xu, Y., Colletier, J. P., Weik, M., Jiang, H., Moult, J., Silman, I., and Sussman, J. L. (2008) Flexibility of aromatic residues in the active-site gorge of acetylcholinesterase: X-ray versus molecular dynamics. *Biophys. J. 95*, 2500−2511.
(45) Harel, M., Sussman, J. L., Krejci, E., Bon, S., Chanal, P., Massoulie, J., and Silman, I. (1992) Conversion of acetylcholinesterase to butyrylcholinesterase: modeling and mutagenesis. *Proc. Natl. Acad. Sci. U.S.A. 89*, 10827−10831.
(46) Ordentlich, A., Barak, D., Kronman, C., Flashner, Y., Leitner, M., Segall, Y., Ariel, N., Cohen, S., Velan, B., and Shafferman, A. (1993) Dissection of the human acetylcholinesterase active center determinants of substrate specificity. Identification of residues constituting the anionic site, the hydrophobic site, and the acyl pocket. *J. Biol. Chem. 268*, 17083−17095.
(47) Masson, P., Nachon, F., and Lockridge, O. (2010) Structural approach to the aging of phosphylated cholinesterases. *Chem.-Biol. Interact. 187*, 157−162.
(48) Nachon, F., Carletti, E., Worek, F., and Masson, P. (2010) Aging mechanism of butyrylcholinesterase inhibited by an N-methyl analogue of tabun: implications of the trigonal-bipyramidal transition state rearrangement for the phosphylation or reactivation of cholinesterases. *Chem.-Biol. Interact. 187*, 44−48.